

Balanced Multimodal Learning via Mutual Information

Rongrong Xie and Guido Sanguinetti

Scuola Internazionale Superiore di Studi Avanzati (SISSA)

Abstract

Multimodal learning has increasingly become a focal point in research, primarily due to its ability to integrate complementary information from diverse modalities. Nevertheless, modality imbalance, stemming from factors such as insufficient data acquisition and disparities in data quality, has often been inadequately addressed. This issue is particularly prominent in biological data analysis, where datasets are frequently limited, costly to acquire, and inherently heterogeneous in quality. Conventional multimodal methodologies typically fall short in concurrently harnessing intermodal synergies and effectively resolving modality conflicts.

In this study, we propose a novel unified framework explicitly designed to address modality imbalance by utilizing mutual information to quantify interactions between modalities. Our approach adopts a balanced multimodal learning strategy comprising two key stages: cross-modal knowledge distillation (KD) and a multitask-like training paradigm. During the cross-modal KD pretraining phase, stronger modalities are leveraged to enhance the predictive capabilities of weaker modalities. Subsequently, our primary training phase employs a multitask-like learning mechanism, dynamically calibrating gradient contributions based on modality-specific performance metrics and intermodal mutual information. This approach effectively alleviates modality imbalance, thereby significantly improving overall multimodal model performance.

1 Introduction

Multimodal learning aims to integrate complementary signals from diverse data types, yet in practice one modality often dominates training when information content, data quality, or sample size are imbalanced. This *modality imbalance* suppresses the benefits of integration and is especially problematic in biomedical applications such as multi-omics disease subtyping, where cohorts are small and assays vary in noise and coverage. Foundational syntheses emphasize fusion, alignment, and coordination as core challenges, but principled mechanisms that explicitly counter modality imbalance while preserving useful cross-modal structure remain limited [Baltrušaitis et al., 2018].

We propose a balanced multimodal framework for multi-omics classification that combines three ideas: (i) graph-based encoders that exploit cross-sample structure; (ii) cross-modal knowledge transfer to strengthen weaker modalities; and (iii) a multitask-style optimization procedure that adaptively reweights unimodal and multimodal losses based on performance signals and cross-modal dependence. Concretely, we employ a revised graph convolutional encoder in which node features may derive from a single modality, while edges are constructed from a fused similarity network across modalities. We then pretrain weaker modalities via *knowledge distillation* from a stronger teacher to transfer predictive structure without overfitting [Hinton et al., 2015, Furlanello et al., 2018]. Finally, we train the joint model with dynamic loss balancing so that no single modality dictates the gradients, leveraging advances in multitask optimization [Chen et al., 2018, Kendall et al., 2018].

A central component of our approach is quantifying and utilizing cross-modal statistical dependence. We use mutual information (MI) both to guide when knowledge transfer is plausible and to modulate training so that fusion emphasizes informative relations. Modern MI estimators (e.g., MINE) and InfoNCE-style contrastive objectives make such dependence measurable and tractable in deep models, and MI maximization has improved multimodal fusion in prior work [Belghazi et al., 2018, Oord et al., 2018, Han et al., 2021].

We evaluate our method on breast cancer (BRCA) classification using copy-number variation (CNV), mRNA expression, and proteomic (RPPA) profiles assembled from community resources that promote reproducibility (UCSC Xena and TCPA) [Goldman et al., 2020, Li et al., 2017]. Across experiments, the combination of fused-graph encoders, MI-aware distillation, and adaptive reweighting mitigates modality imbalance and improves macro-F1 relative to naive early/late fusion and unimodal baselines, while remaining robust under low-information channels and small-sample regimes common in oncology.

More broadly, our results suggest a practical recipe for multimodal learning under scarcity and heterogeneity: *transfer what is reliable, quantify what is shared, and balance what is optimized*. Although we focus on bulk multi-omics, the same principles extend to other settings (e.g., single-cell multi-omics, imaging-genomics, or clinical multimodal records) and can be coupled with probabilistic integration frameworks (e.g., MOFA+) to accommodate missingness and uncertainty [Argelaguet et al., 2020].

2 Method

2.1 Overall Framework and Problem Formulation

Integrating multi-omics data for classification tasks is challenging due to the inherent imbalance and varying levels of informativeness among different data modalities. Consider a dataset with N samples, each represented across M modalities denoted as $X = \{X^1, X^2, \dots, X^m, \dots, X^M\}$. All modalities share the same ground truth label y among C distinct classes. Our goal is to develop a robust classification framework that effectively leverages all modalities while addressing the imbalance problem.

To achieve this, we propose a unified framework that incorporates a revised Graph Convolutional Network (r-GCN) as the unimodal encoder for each modality (illustrated in Figure 1). Detailed in Section 2.2, this r-GCN enhances feature representations by integrating multi-modal similarities into its graph structure, enabling each modality to capture more informative and discriminative patterns. Alongside the r-GCN, our framework addresses modality imbalance through two key strategies, elaborated in Section 2.3: (1) Self-Distillation Pretraining, where weaker modalities learn from stronger ones by distilling knowledge from their pretrained models, and (2) a Multitask-Like Learning Framework that dynamically adjusts the learning contributions of each modality based on performance metrics such as the macro F1 score.

2.2 revised Graph Convolution Network

Similarity Network Fusion Similarity Network Fusion [Wang et al., 2014] (SNF) is a computational method used to integrate multiple modalities into a unified network, which is particularly useful in biomedical applications for understanding complex biological systems.

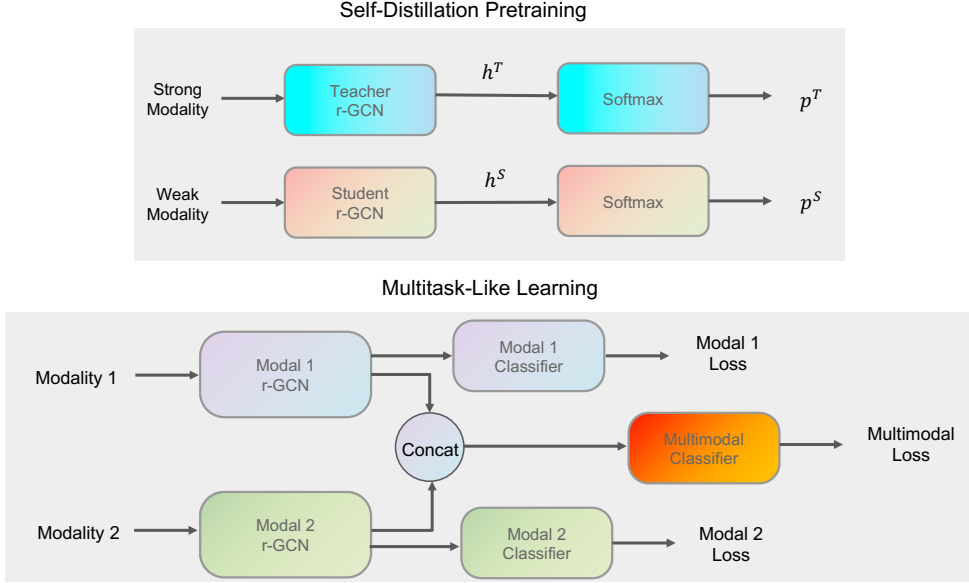


Figure 1: Framework.

When fusing two modalities, SNF begins by constructing a similarity matrix \mathbf{W} for each modality, quantifying the similarity between samples:

$$\mathbf{W}(i, j) = \exp\left(-\frac{\rho^2(x_i, x_j)}{\mu \epsilon_{i,j}}\right), \quad (1)$$

where $\rho(x_i, x_j)$ is the Euclidean distance between samples x_i and x_j , μ is a hyperparameter, and $\epsilon_{i,j}$ adjusts for scaling effects.

A normalized matrix \mathbf{P} is then defined:

$$\mathbf{P}(i, j) = \begin{cases} \frac{\mathbf{W}(i, j)}{2 \sum_{k \neq i} \mathbf{W}(i, k)}, & \text{if } j \neq i \\ \frac{1}{2}, & \text{if } j = i \end{cases}$$

To emphasize local similarities, a K -nearest neighbors matrix \mathbf{S} is computed:

$$\mathbf{S}(i, j) = \begin{cases} \frac{\mathbf{W}(i, j)}{\sum_{k \in N_i} \mathbf{W}(i, k)}, & \text{if } j \in N_i \\ 0, & \text{otherwise} \end{cases}$$

where N_i contains the K nearest neighbors of sample i .

The fusion process iteratively updates the similarity matrices:

$$\begin{aligned} \mathbf{P}_{t+1}^1 &= \mathbf{S}^1 \mathbf{P}_t^2 (\mathbf{S}^1)^\top, \\ \mathbf{P}_{t+1}^2 &= \mathbf{S}^2 \mathbf{P}_t^1 (\mathbf{S}^2)^\top. \end{aligned}$$

Here, \mathbf{P}_t^1 and \mathbf{P}_t^2 represent the status matrices for the first and second modalities, respectively, at iteration t .

After convergence, the integrated network is obtained by averaging:

$$\mathbf{P}^c = \frac{\mathbf{P}_t^1 + \mathbf{P}_t^2}{2}. \quad (2)$$

This results in a unified similarity matrix that effectively combines multiple modalities, enhancing the representation of relationships among samples.

Graph Convolutional Networks Graph Convolutional Networks [Kipf and Welling, 2016] (GCNs) have become a fundamental framework for analyzing graph-structured data, allowing for the extraction of salient patterns and representations through the simultaneous utilization of node features and the graph topology. The training of a GCN model requires two essential inputs: the feature matrix $X \in \mathbb{R}^{N \times B}$, where N denotes the number of nodes and B represents the dimensionality of the feature space associated with each node, and the adjacency matrix $A \in \mathbb{R}^{N \times N}$, which encapsulates the graph’s structural information.

The GCN architecture typically consists of multiple convolutional layers. The propagation rule for the l -th layer is expressed as:

$$H^{(l+1)} = \sigma \left(\tilde{D}^{-\frac{1}{2}} (\tilde{A}) \tilde{D}^{-\frac{1}{2}} H^{(l)} W^{(l)} \right),$$

where $\tilde{A} = A + I_N$ is the adjacency matrix with added self-loops, I_N is the identity matrix of size N , \tilde{D} represents the corresponding degree matrix, and $W^{(l)}$ is the trainable weight matrix at layer l . The function σ is the non-linear activation function, typically the Rectified Linear Unit (ReLU).

In this formulation, the input to each layer $H^{(l)}$ is iteratively updated, with the initial input $H^{(0)}$ set to the feature matrix X . This propagation mechanism enables GCNs to effectively integrate and transform node features across the graph, capturing both local neighborhood information and broader structural patterns.

For datasets lacking a predefined adjacency matrix, the adjacency element A_{ij} between nodes i and j can be computed as follows:

$$A_{ij} = \begin{cases} s(\mathbf{x}_i, \mathbf{x}_j), & \text{if } i \neq j \text{ and } s(\mathbf{x}_i, \mathbf{x}_j) \geq \epsilon, \\ 0, & \text{otherwise,} \end{cases}$$

where \mathbf{x}_i and \mathbf{x}_j are the feature vectors corresponding to nodes i and j , respectively. For unimodal, the similarity network $s(\mathbf{x}_i, \mathbf{x}_j)$ can be computed using the scaled exponential similarity, as given in Eq.(1). For multimodal, the similarity can be derived via the SNF algorithm, detailed in Eq.(2). The threshold ϵ is typically determined based on the desired average number of edges per node [Wang et al., 2021].

revised Graph Convolution Network As previously discussed, GCNs utilize node features and the relationships between nodes, often represented by a similarity matrix, to perform various tasks. However, in the context of biological data, such as transcriptomic data, we have observed that the similarity matrix often exhibits low values, which fails to effectively capture the relationships between nodes.

In response to this limitation, we propose a revised GCN (r-GCN) approach wherein the strict relationship between nodes and edges is relaxed. In this revised model, node features may originate from a single modality, while edge weights are derived from a similarity matrix that integrates multiple modalities. This integration is achieved using the SNF algorithm, thereby enhancing the representation of relationships in the network.

2.3 Balanced Multimodal Learning

Imbalanced multimodal learning remains a significant challenge due to the varying levels of informativeness and performance across different modalities. Current methods typically address this issue by either controlling the training of unimodal encoders based on inter-modal performance discrepancies or by reducing the impact of low-informative modalities. In this paper, we present a novel and comprehensive methodology that integrates both aspects. Initially, we utilize the macro F1 score to assess the learning state of each modality, categorizing them into strong, weak, or low-information groups. We then employ self-distillation to pre-train the modalities, allowing weaker modalities to benefit from the knowledge of stronger ones. Finally, we apply a multitask-like multimodal framework that dynamically adjusts the gradient magnitudes for each modality, ensuring a balanced and effective multimodal learning process.

2.3.1 Estimating the Modality Learning State

To evaluate the learning state of each modality, we employ the *macro F1 score* due to its robustness and straightforward application.

Previous approaches have often estimated unimodal learning states by analyzing differences between training and validation datasets. For example, [Wang et al., 2020] utilized the *overfitting-to-generalization ratio*, calculated from the training loss L^{Tr} and validation loss L^{Va} at epochs e and $e + n$:

$$O_e = L_e^{Va} - L_e^{Tr}, \quad \text{Ratio} = \left| \frac{O_{e+n} - O_e}{L_e^{Va} - L_{e+n}^{Va}} \right|.$$

Similarly, [Wei et al., 2024] proposed the *purity gap* g^m , defined as the difference between the training purity P_{Tr}^m and validation purity P_{Va}^m , where purity measures how well the representations cluster according to the true class labels.

However, in our experiments with omics data, we found that these metrics did not effectively reflect the true learning states of different modalities. Specifically, the overfitting-to-generalization ratio and purity gap yielded similar values across modalities, despite variations in their actual performance. This indicates that these metrics are insufficiently sensitive to the nuances of each modality’s learning process, limiting their utility in our context.

In contrast, the macro F1 score overcomes these limitations by providing a straightforward and accurate measure of each modality’s true performance. Furthermore, unlike the softmax-based prediction scores of each modality [Peng et al., 2022], it offers a balanced evaluation even in datasets with class imbalances. Therefore, we advocate for the use of the macro F1 score as a more reliable and effective metric for estimating unimodal learning states in multimodal learning settings with imbalanced datasets.

2.3.2 Multimodal Pre-training with Self-Distillation

To address the challenge of imbalanced multimodal learning, we employ a self-distillation strategy [Liu et al., 2023] to transfer knowledge from a strong modality to a weaker one during pre-training. This approach leverages the rich information captured by the strong modality to enhance the learning of the weaker modality.

We designate the modality with the highest macro F1 score as the *strong modality*. If a modality’s macro F1 score is close to that of random guessing, i.e., $1/C$ where C is the number of classes, it indicates that it contains very little useful information; we refer to it as a *low-information modality*. Modalities with macro F1 scores between the strong modality and the low-information modality are termed *weak modalities*. In this work, we apply self-distillation to improve the performance of weak modalities with the assistance of the strong modality. The details are illustrated in Figure 1.

We first pre-train a teacher model using the strong modality. For each sample i in the strong modality, the teacher model extracts a representation h_i^T . The predictions for the C classes are obtained by applying the SoftMax function to h_i^T , i.e.,

$$p_i^T = \frac{e^{h_i^T}}{\sum_{j=1}^C e^{h_j^T}}.$$

After pre-training the teacher model, we train a student model using the weak modality. During training, the loss function L is defined as:

$$\begin{aligned} L &= \alpha_1 L_{CE} + \alpha_2 L_{KL} + \alpha_3 L_{RE}, \\ L_{CE} &= - \sum_{i=1}^N y_i^S \log p_i^S, \\ L_{KL} &= \sum_{i=1}^N D_{KL}(p_i^T \| p_i^S), \\ L_{RE} &= \sum_{i=1}^N \frac{\|h_i^T - h_i^S\|^2}{d}. \end{aligned}$$

Here, L_{CE} computes the cross-entropy loss for the student model, where y_i^S is the true label for sample i and p_i^S is the predicted probability from the student model. The terms L_{KL} and L_{RE} are the self-distillation components, where the student model attempts to mimic the knowledge (prediction distributions and representations) of the teacher model. Specifically, L_{KL} is the Kullback–Leibler divergence between the teacher’s predicted probabilities p_i^T and the student’s predicted probabilities p_i^S . The term L_{RE} is the Euclidean distance between the representations of the teacher model h_i^T and the student model h_i^S , normalized by the dimension d of the representations. The weighting factors α_1 , α_2 , and α_3 are used to balance the contributions of each loss component.

We refrain from applying self-distillation strategies to low-information modalities because they have limited capacity and low correlation with the strong modality. However, if a low-information modality exhibits sufficient correlation with the strong modality—such as a mutual information greater than 0.2—it can still benefit from the self-distillation strategy.

2.3.3 Multitask-like Multimodal Framework

After utilizing self-distillation for pre-training the modalities, we employ a multitask-like multimodal framework [Wang et al., 2020] to further address the issue of imbalanced multimodal learning. In the multitask-like framework illustrated in Figure 1, each modality \mathbf{X}^m is fed into its corresponding encoder $\varphi^m(\mathbf{X}^m)$ parameterized by θ^m to extract features. These extracted features are then fused using a fusion operation \oplus (e.g., concatenation) and passed to a multimodal classifier $f^{M+1}(\varphi^1 \oplus \varphi^2 \oplus \dots \oplus \varphi^M)$, where $M + 1$ denotes the multimodal classifier.

Simultaneously, the features from each modality’s encoder $\varphi^m(\mathbf{X}^m)$ are also passed to their respective unimodal classifiers $f^m(\varphi^m(\mathbf{X}^m))$. In this multitask-like multimodal framework, we consider not only the multimodal loss $L^{M+1} = L(f^{M+1}(\varphi^1 \oplus \varphi^2 \oplus \dots \oplus \varphi^M), y)$ but also the optimization of each unimodal classifier, incorporating the unimodal losses $L^m = L(f^m(\varphi^m(\mathbf{X}^m)), y)$ for $m = 1, \dots, M + 1$. Therefore, the total loss of the model is:

$$L = \sum_{m=1}^{M+1} k_t^m L^m,$$

where k_t^m is a coefficient used to reweight each loss term. By reweighting the losses, we can control the magnitude of gradients from each task (both multimodal and unimodal), thereby reducing gradient conflicts. This balancing mechanism leads to more synergistic updates and has been empirically verified to effectively alleviate the imbalanced multimodal learning problem [Wei and Hu, 2024].

Regarding the definition of the coefficient k_t^m , previous works often focus either on dominant and weak modalities [Peng et al., 2022, Kontras et al., 2024] or on low-information modalities [Wei et al., 2024]. In contrast, we propose a novel and more comprehensive approach that combines both considerations. We define k_t^m as follows:

$$r_t^m = \frac{F^m}{\frac{1}{M-1} \sum_{j=1, j \neq m}^M F^j},$$

$$k_t^m = \begin{cases} 1 - \tanh(\alpha \cdot r_t^m), & \text{if } F^m > \gamma \frac{1}{C}, \\ \tanh(\beta \cdot r_t^m), & \text{otherwise,} \end{cases}$$

where F^m is the macro F1 score of modality m , r_t^m is the ratio of the macro F1 score of modality m compared to the average macro F1 score of the other modalities, and \tanh provides a smooth normalization of r_t^m . The parameters α , β , and γ are hyperparameters.

By defining k_t^m in this manner, we ensure that low-information modalities receive a lower weighting (by setting a small β), thereby decreasing their contribution to the overall loss and preventing them from adversely affecting the model’s performance. Additionally, this approach decreases the weight of strong modalities and increases the weight of weak modalities, mitigating the dominance of strong modalities in the optimization process. Consequently, weaker modalities receive sufficient optimization efforts, allowing them to gain adequate training.

3 Experiment

3.1 Dataset and implementation details

In this study, we utilize the BRCA dataset, accessible via the UCSC Xena browser (<https://xenabrowser.net/>) and the Cancer Proteome Atlas (TCPA) portal (<https://tcpaportal.org/tcpa/>). This dataset, fo-

Table 1: The number of samples for each subtype of BRCA.

| | Basal-like | Her2-enriched | Luminal A | Luminal B | Total |
|-------------------|------------|---------------|-----------|-----------|-------|
| Number of samples | 112 | 53 | 248 | 98 | 511 |

Table 2: The number of features for each modality of BRCA.

| | mRNA | CNV | RPPA |
|--------------------|-------|-------|------|
| Number of features | 19580 | 19273 | 223 |

cused on breast tumors, encompasses four distinct molecular subtypes: (1) Basal-like, characterized by the absence of hormone receptor and ERBB2 expression; (2) HER2-enriched, notable for its over-expression of the oncogene ERBB2; (3) Luminal A; and (4) Luminal B. Both Luminal A and B subtypes are generally estrogen receptor (ER)-positive and express epithelial markers, although Luminal B exhibits a higher Ki67 index and a less favorable prognosis compared to Luminal A. For our analysis, we selected multi-omic data across three biological levels: genomic (copy number variation, CNV), transcriptomic (mRNA sequencing), and proteomic (reverse phase protein array, RPPA). A total of 511 patients with data available across all three omics were included in the study. Detailed information regarding the dataset is provided in Table 1.

3.2 Baseline

The dimensional characteristics of each modality within the BRCA dataset are presented in Table 2. Given the high dimensionality of this data, substantial computational resources are required for analysis. To mitigate the computational burden, we employed an autoencoder to reduce the dimensionality of each modality to 100 features. Recognizing that different modalities may exhibit varying levels of classification performance, we utilized a random forest classifier as a benchmark to evaluate and compare the classification performance of individual modalities as well as various combinations of these modalities, see the accuracy, roc-auc, and average f1 results in Table 3.

Based on Table 3, it is evident that the classification performance of the CNV modality is significantly lower compared to mRNA and RPPA across all metrics, including accuracy, AUC, and Macro F1. When CNV is combined with other modalities, the performance improvements are minimal or, in some cases, even result in a decrease compared to combinations that exclude CNV. This suggests a clear imbalance among the modalities. The CNV modality appears to introduce a substantial amount of noise, which adversely affects the model’s predictive capability, leading to poorer overall performance. Therefore, if the noise inherent in the CNV modality is not appropriately addressed, and all modalities are combined indiscriminately for classification tasks, the expected improvement in classification performance may not be realized, and it may, in fact, deteriorate.

3.3 revised Graph convolution network

We view each sample as a node within a graph, wherein both the node features and the inter-nodal relationships—established via a similarity network—are input into a GCN to perform classification tasks. As illustrated in Table 4, two distinct types of node features are considered: single modality and combined modalities. For the single modality, we employ a scaled exponential similarity algorithm to construct a weighted similarity network. In contrast, for the combined modalities, we

Table 3: Classification performance across various modalities using the logistic regression.

| | Accuracy | AUC | Macro F1 |
|---------------|---------------------|---------------------|---------------------|
| mRNA | 0.8338 ± 0.0340 | 0.9510 ± 0.0115 | 0.7476 ± 0.0504 |
| CNV | 0.5831 ± 0.0338 | 0.6763 ± 0.0221 | 0.3206 ± 0.0168 |
| RPPA | 0.8434 ± 0.0231 | 0.9602 ± 0.0067 | 0.8130 ± 0.0282 |
| mRNA+CNV | 0.8338 ± 0.0354 | 0.9503 ± 0.0090 | 0.7576 ± 0.0412 |
| RPPA+CNV | 0.8493 ± 0.0203 | 0.9603 ± 0.0065 | 0.8233 ± 0.0201 |
| RPPA+mRNA | 0.8728 ± 0.0156 | 0.9737 ± 0.0050 | 0.8403 ± 0.0249 |
| RPPA+mRNA+CNV | 0.8728 ± 0.0174 | 0.9735 ± 0.0053 | 0.8367 ± 0.0292 |

Table 4: Classification performance across various modalities using the graph convolution network.

| | Accuracy | AUC | Macro F1 |
|---------------------|----------|--------|----------|
| Node: mRNA | 0.8727 | 0.9528 | 0.8248 |
| Edge: mRNA | | | |
| Node: CNV | 0.6066 | 0.7172 | 0.3428 |
| Edge: CNV | | | |
| Node: RPPA | 0.8865 | 0.9658 | 0.8607 |
| Edge: RPPA | | | |
| Node: mRNA+CNV | 0.8767 | 0.9593 | 0.8318 |
| Edge: mRNA+CNV | | | |
| Node: mRNA+RPPA | 0.9061 | 0.9838 | 0.8905 |
| Edge: mRNA+RPPA | | | |
| Node: CNV+RPPA | 0.8727 | 0.9623 | 0.8464 |
| Edge: CNV+RPPA | | | |
| Node: mRNA+CNV+RPPA | 0.9178 | 0.9840 | 0.9051 |
| Edge: mRNA+CNV+RPPA | | | |

utilize the SNF algorithm to generate a fusion-weighted similarity network.

The results presented in Table 4 indicate that the GCN outperforms the random forest algorithm in classification accuracy. Nonetheless, as depicted in Figure 2, the patient similarities within the single modality similarity network exhibit weaker associations (i.e., low-weight edges) when compared to those observed in the fusion-weighted similarity network generated via SNF. This discrepancy raises our concerns regarding the effectiveness of the single modality similarity network in accurately representing the relationships between samples.

To address this issue, we propose a revised GCN algorithm wherein the similarity network is consistently the fusion similarity network, irrespective of the input features. This adjustment ensures a more robust representation of sample relationships. As evidenced by the results in Table 5 and Figure 3, this revised GCN outperforms both the original GCN and the random forest algorithm. Nevertheless, it is important to note that across all algorithms, the inclusion of CNV as a modality in the combined input consistently leads to a decline in model performance.

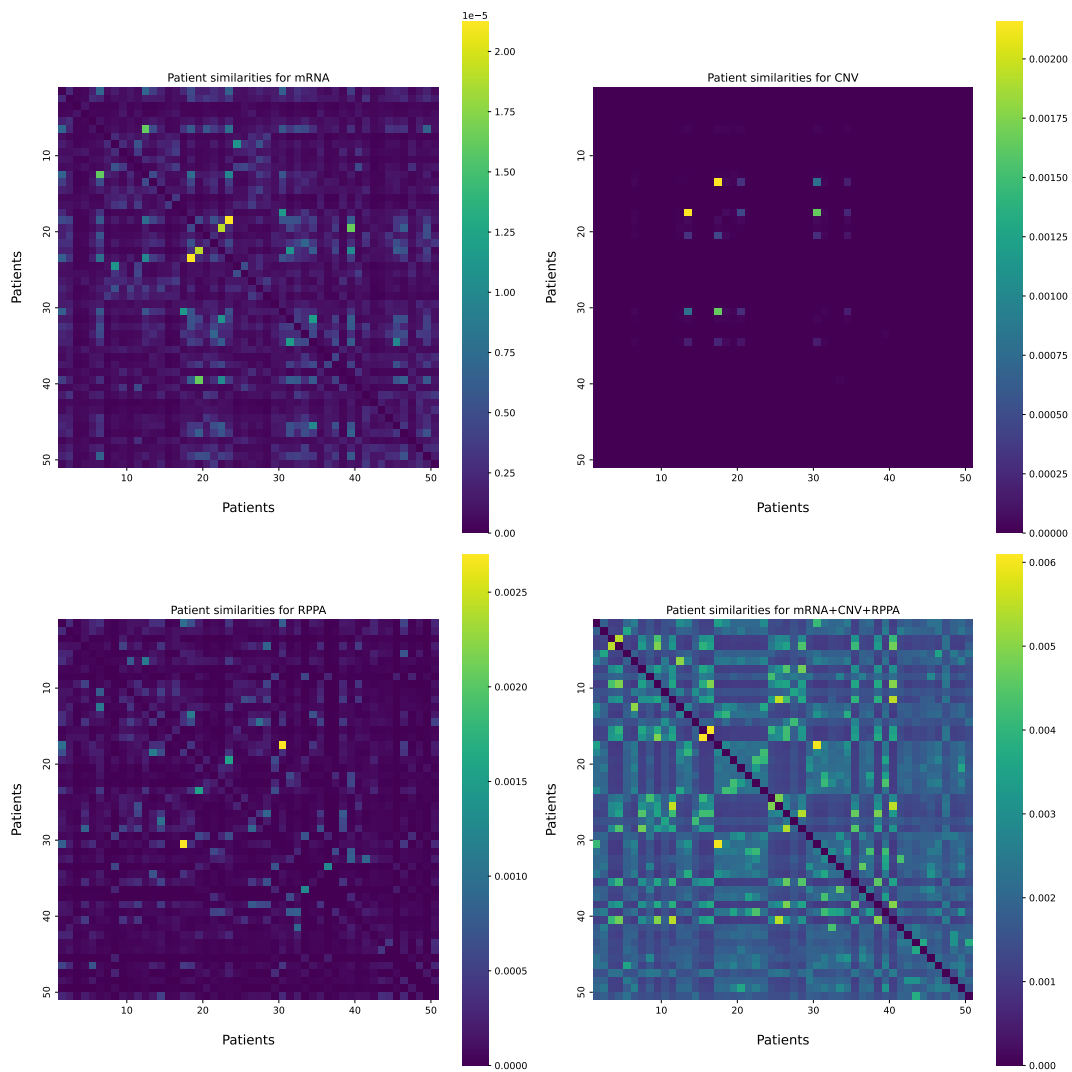


Figure 2: Heatmap comparison across various modalities.

Table 5: Classification performance across various modalities using the revised graph convolution network.

| | Accuracy | AUC | Macro F1 |
|---------------------|----------|--------|----------|
| Node: mRNA | 0.8747 | 0.9592 | 0.8314 |
| Edge: mRNA+CNV+RPPA | | | |
| Node: CNV | 0.6438 | 0.7836 | 0.3730 |
| Edge: mRNA+CNV+RPPA | | | |
| Node: RPPA | 0.9001 | 0.9773 | 0.8820 |
| Edge: mRNA+CNV+RPPA | | | |
| Node: mRNA+CNV | 0.8786 | 0.9645 | 0.8328 |
| Edge: mRNA+CNV+RPPA | | | |
| Node: mRNA+RPPA | 0.9178 | 0.9848 | 0.9143 |
| Edge: mRNA+CNV+RPPA | | | |
| Node: CNV+RPPA | 0.9021 | 0.9768 | 0.8840 |
| Edge: mRNA+CNV+RPPA | | | |

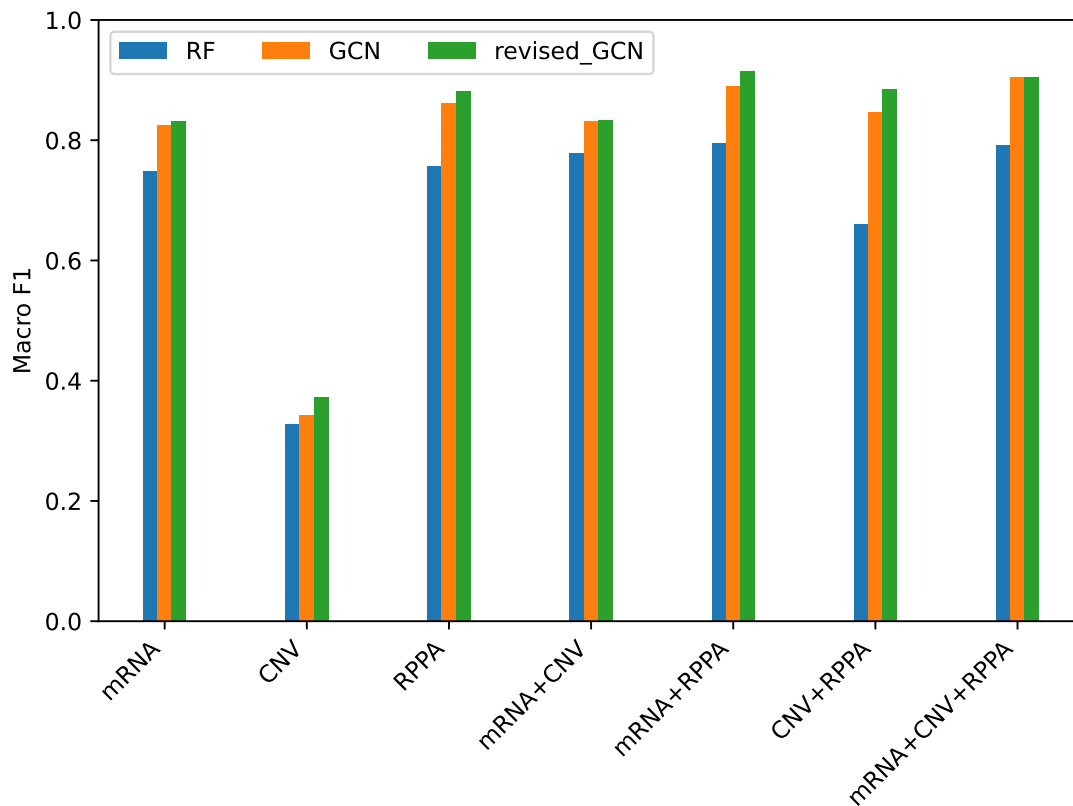


Figure 3: Classification performance of different algorithms across various modalities.

4 Conclusion

We presented a balanced multimodal learning framework that unifies (1) an r-GCN encoder leveraging cross-modal similarity networks, (2) cross-modal self-distillation to elevate weak modalities, and (3) a multitask-like training scheme that reweights losses using macro-F1 and mutual information. On multi-omics BRCA classification, our framework alleviates dominance by strong modalities, suppresses the influence of low-information channels, and yields consistent performance gains over standard concatenation and unimodal models. Beyond the specific application, our results support a general recipe for multimodal learning under data scarcity and heterogeneity: **transfer what is reliable, quantify what is shared, and balance what is optimized**. Future work will extend our framework to settings with systematically missing modalities, explore alternative dependence measures beyond MI (e.g., Wasserstein-based criteria), and integrate uncertainty-aware task weighting to further stabilize training in ultra-low-sample cohorts.

References

- [Argelaguet et al., 2020] Argelaguet, R., Arnol, D., Bredikhin, D., Deloro, Y., Velten, B., Marioni, J. C., and Stegle, O. (2020). Mofa+: a statistical framework for comprehensive integration of multi-modal single-cell data. *Genome biology*, 21(1):111.
- [Baltrušaitis et al., 2018] Baltrušaitis, T., Ahuja, C., and Morency, L.-P. (2018). Multimodal machine learning: A survey and taxonomy. *IEEE transactions on pattern analysis and machine intelligence*, 41(2):423–443.
- [Belghazi et al., 2018] Belghazi, M. I., Baratin, A., Rajeshwar, S., Ozair, S., Bengio, Y., Courville, A., and Hjelm, D. (2018). Mutual information neural estimation. In *International conference on machine learning*, pages 531–540. PMLR.
- [Chen et al., 2018] Chen, Z., Badrinarayanan, V., Lee, C.-Y., and Rabinovich, A. (2018). Grad-norm: Gradient normalization for adaptive loss balancing in deep multitask networks. In *International conference on machine learning*, pages 794–803. PMLR.
- [Furlanello et al., 2018] Furlanello, T., Lipton, Z., Tschannen, M., Itti, L., and Anandkumar, A. (2018). Born again neural networks. In *International conference on machine learning*, pages 1607–1616. PMLR.
- [Goldman et al., 2020] Goldman, M. J., Craft, B., Hastie, M., Repčeka, K., McDade, F., Kamath, A., Banerjee, A., Luo, Y., Rogers, D., Brooks, A. N., et al. (2020). Visualizing and interpreting cancer genomics data via the xena platform. *Nature biotechnology*, 38(6):675–678.
- [Han et al., 2021] Han, W., Chen, H., and Poria, S. (2021). Improving multimodal fusion with hierarchical mutual information maximization for multimodal sentiment analysis. *arXiv preprint arXiv:2109.00412*.
- [Hinton et al., 2015] Hinton, G., Vinyals, O., and Dean, J. (2015). Distilling the knowledge in a neural network. *arXiv preprint arXiv:1503.02531*.

- [Kendall et al., 2018] Kendall, A., Gal, Y., and Cipolla, R. (2018). Multi-task learning using uncertainty to weigh losses for scene geometry and semantics. In *Proceedings of the IEEE conference on computer vision and pattern recognition*, pages 7482–7491.
- [Kipf and Welling, 2016] Kipf, T. N. and Welling, M. (2016). Semi-supervised classification with graph convolutional networks. *arXiv preprint arXiv:1609.02907*.
- [Kontras et al., 2024] Kontras, K., Chatzichristos, C., Blaschko, M., and De Vos, M. (2024). Improving multimodal learning with multi-loss gradient modulation. *arXiv preprint arXiv:2405.07930*.
- [Li et al., 2017] Li, J., Akbani, R., Zhao, W., Lu, Y., Weinstein, J. N., Mills, G. B., and Liang, H. (2017). Explore, visualize, and analyze functional cancer proteomic data using the cancer proteome atlas. *Cancer research*, 77(21):e51–e54.
- [Liu et al., 2023] Liu, S., Li, L., Song, J., Yang, Y., and Zeng, X. (2023). Multimodal pre-training with self-distillation for product understanding in e-commerce. In *Proceedings of the Sixteenth ACM International Conference on Web Search and Data Mining*, pages 1039–1047.
- [Oord et al., 2018] Oord, A. v. d., Li, Y., and Vinyals, O. (2018). Representation learning with contrastive predictive coding. *arXiv preprint arXiv:1807.03748*.
- [Peng et al., 2022] Peng, X., Wei, Y., Deng, A., Wang, D., and Hu, D. (2022). Balanced multimodal learning via on-the-fly gradient modulation. In *Proceedings of the IEEE/CVF conference on computer vision and pattern recognition*, pages 8238–8247.
- [Wang et al., 2014] Wang, B., Mezlini, A. M., Demir, F., Fiume, M., Tu, Z., Brudno, M., Haibe-Kains, B., and Goldenberg, A. (2014). Similarity network fusion for aggregating data types on a genomic scale. *Nature methods*, 11(3):333–337.
- [Wang et al., 2021] Wang, T., Shao, W., Huang, Z., Tang, H., Zhang, J., Ding, Z., and Huang, K. (2021). Mogonet integrates multi-omics data using graph convolutional networks allowing patient classification and biomarker identification. *Nature communications*, 12(1):3445.
- [Wang et al., 2020] Wang, W., Tran, D., and Feiszli, M. (2020). What makes training multi-modal classification networks hard? In *Proceedings of the IEEE/CVF conference on computer vision and pattern recognition*, pages 12695–12705.
- [Wei and Hu, 2024] Wei, Y. and Hu, D. (2024). Mmpareto: Boosting multimodal learning with innocent unimodal assistance. *arXiv preprint arXiv:2405.17730*.
- [Wei et al., 2024] Wei, Y., Li, S., Feng, R., and Hu, D. (2024). Diagnosing and re-learning for balanced multimodal learning. *arXiv preprint arXiv:2407.09705*.